Wireless, soft electronics for rapid, multisensor measurements of hydration levels in healthy and diseased skin

Kyeongha Kwon[a,b,1], Heling Wang[c,d,e,1], Jaeman Lim[a,f], Keum San Chun[g], Hokyung Jang[h], Injae Yoo[b], Derek Wu[a,e], Alyssa Jie Chen[a], Carol Ge Gu[a], Lindsay Lipschultz[i], Jong Uk Kim[j], Jihye Kim[a,k], Hyoyoung Jeong[a], Haiwen Luan[a,c,d,e], Yoonseok Park[a], Chun-Ju Su[a], Yui Ishida[l], Surabhi R. Madhvapathy[a,d], Akihiko Ikoma[l], Jean Won Kwak[a,e], Da Som Yang[a], Anthony Banks[a], Shuai Xu[a,i,m], Yonggang Huang[c,d,e], Jan-Kai Chang[a,f,2], and John A. Rogers[a,d,e,i,n,o,p,q,2]

[a]Querrey-Simpson Institute for Bioelectronics, Northwestern University, Evanston, IL 60208; [b]School of Electrical Engineering, Korea Advanced Institute of Science and Technology, 34141 Daejeon, Republic of Korea; [c]Department of Civil and Environmental Engineering, Northwestern University, Evanston, IL 60208; [d]Department of Materials Science and Engineering, Northwestern University, Evanston, IL 60208; [e]Department of Mechanical Engineering, Northwestern University, Evanston, IL 60208; [f]Wearifi Inc., Evanston, IL 60201; [g]Electrical and Computer Engineering, The University of Texas at Austin, Austin, TX 78712; [h]Department of Electrical and Computer Engineering, University of Wisconsin, Madison, WI 53706; [i]Department of Biomedical Engineering, Northwestern University, Evanston, IL 60208; [j]School of Chemical Engineering, Sungkyunkwan University, 16419 Suwon, Republic of Korea; [k]School of Advanced Materials Science and Engineering, Sungkyunkwan University, 16419 Suwon, Republic of Korea; [l]Maruho Co., Ltd., 531-0071 Osaka, Japan; [m]Department of Dermatology, Feinberg School of Medicine, Northwestern University, Chicago, IL 60611; [n]Department of Neurological Surgery, Northwestern University, Chicago, IL 60611; [o]Department of Chemistry, Northwestern University, Evanston, IL 60208; [p]Department of Chemical Engineering, Northwestern University, Evanston, IL 60208; and [q]Department of Electrical Engineering and Computer Science, Northwestern University, Evanston, IL 60208

Contributed by John A. Rogers, December 8, 2020 (sent for review October 16, 2020; reviewed by Tsuyoshi Sekitani and Benjamin C. K. Tee)

Precise, quantitative measurements of the hydration status of skin can yield important insights into dermatological health and skin structure and function, with additional relevance to essential processes of thermoregulation and other features of basic physiology. Existing tools for determining skin water content exploit surrogate electrical assessments performed with bulky, rigid, and expensive instruments that are difficult to use in a repeatable manner. Recent alternatives exploit thermal measurements using soft wireless devices that adhere gently and noninvasively to the surface of the skin, but with limited operating range (~1 cm) and high sensitivity to subtle environmental fluctuations. This paper introduces a set of ideas and technologies that overcome these drawbacks to enable high-speed, robust, long-range automated measurements of thermal transport properties via a miniaturized, multisensor module controlled by a long-range (~10 m) Bluetooth Low Energy system on a chip, with a graphical user interface to standard smartphones. Soft contact to the surface of the skin, with almost zero user burden, yields recordings that can be quantitatively connected to hydration levels of both the epidermis and dermis, using computational modeling techniques, with high levels of repeatability and insensitivity to ambient fluctuations in temperature. Systematic studies of polymers in layered configurations similar to those of human skin, of porcine skin with known levels of hydration, and of human subjects with benchmarks against clinical devices validate the measurement approach and associated sensor hardware. The results support capabilities in characterizing skin barrier function, assessing severity of skin diseases, and evaluating cosmetic and medication efficacy, for use in the clinic or in the home.

wireless electronics | flexible electronics | biomedical devices | health monitoring | diagnostics

Skin, the largest organ of the human body, is a complex, multilayered functional structure that supports an essential collection of protective, sensory, thermoregulatory, and immunological functions (1). A core function of skin is to act as a protective interface to the surrounding environment (2). The three main layers of the skin—stratum corneum (SC), epidermis, and dermis—serve as dynamic physical barriers to exogenous insults and active interfaces to maintain homeostasis. Failure of the protective function can result in a range of deleterious health effects, as an impaired skin barrier can lead to infection, insensible water loss, tissue necrosis, and death (3). Deficiencies in barrier function are also the underlying drivers of atopic dermatitis (AD), commonly known as eczema. AD is the most common inflammatory skin condition, affecting 20% of children

Significance

Wireless electronics for monitoring of skin hydration in a quantitative fashion have broad relevance to our understanding of dermatological health and skin structure in both clinical and home settings. Here, we present a miniaturized, long-range automated system that adheres gently to the skin to yield quantitative recordings of skin water content for both epidermis and dermis. This system supports capabilities in characterizing skin barrier, assessing severity of skin diseases, and evaluating cosmetic and medication efficacy, with high levels of repeatability and insensitivity to ambient. Benchtop and pilot studies on patients with skin diseases highlight key features of these devices and their potential for broad utility in clinical research and in home settings to guide the management of disorders of the skin.

Author contributions: K.K., J.-K.C., and J.A.R. designed research; K.K., H.W., J.L., K.S.C., H. Jang, I.Y., D.W., A.J.C., C.G.G., L.L., J.U.K., J.K., H. Jeong, H.L., Y.P., C.-J.S., J.W.K., D.S.Y., and J.-K.C. performed research; Y.I., S.R.M., A.I., and S.X. provided advice on skin assessment products; K.K., H.W., Y.I., A.I., A.B., S.X., Y.H., J.-K.C., and J.A.R. analyzed data; and K.K., H.W., S.X., J.-K.C., and J.A.R. wrote the paper.

Reviewers: T.S., Osaka University; and B.C.K.T., National University of Singapore.

Competing interest statement: We have some potential commercial interest in the technology introduced in this paper. A.B. and J.A.R. are co-founders and J.-K.C. is an employee of a company, Wearifi Inc., that may wish to pursue commercialization of this technology in the future.

[1]K.K. and H.W. contributed equally to this work.

[2]To whom correspondence may be addressed. Email: jkchang@mywearifi.com or jrogers@northwestern.edu.

This article contains supporting information online at https://www.pnas.org/lookup/suppl/doi:10.1073/pnas.2020398118/-/DCSupplemental.

Published January 18, 2021.

and 3% of adults worldwide (4). Dry skin, or xerosis cutis (XC), is another common skin condition associated with barrier impairment, affecting up to 85% of older adults (5). Skin barrier dysfunction in neonates can also predict for the development of AD in subsequent years (6, 7). These and other types of degradation can also increase the systemic absorption of exogenous chemicals and toxic metals, with serious health sequelae (8, 9).

Quantitative evaluations of skin barrier function can provide essential information to guide clinical decision making. Current methods involve a determination of transepidermal water loss (TEWL) via a measurement of water vapor pressure at the skin surface, or an assessment of the high-frequency electrical properties of the skin itself as a surrogate marker of its water content (10). Existing TEWL instruments and skin capacitance methods are available only as expensive devices (2) whose accuracy can be influenced by small changes in ambient temperature (10), by subtle variations in angle and pressure at the skin interface (11, 12), and by slight user-related differences in testing protocols (13). Such limitations confine these methods to use in highly controlled clinical and research studies (14, 15). As an alternative, recent research demonstrates that transient plane source (TPS) methods can be adapted for noninvasive measurements of thermal transport properties of the skin (16–21), where simple models quantitatively connect the thermal properties of the skin to its hydration level (16, 17). The following presents wireless systems for performing such measurements routinely and reliably. Computational methods applied to the resulting data define the hydration levels using bilayer models for the skin, with clinical-grade levels of accuracy. Relative to other recently described technologies (18), important advances include 1) long-range wireless capabilities and high sampling rates with Bluetooth interfaces to the phone; 2) compact, dual-sided multisensor designs with enhanced sensitivity to the hydration levels of the skin; 3) multiple, redundant measurement modalities with minimized susceptibility to parasitic environmental, physiological, and user-related factors; and 4) full-waveform data analysis techniques with ability to determine hydration levels of both the epidermis and dermis, and with additional sensitivity to the SC. Numerical modeling results and benchtop characterization tests under various practical conditions define the key physical effects and guide the selection of optimized designs and modes of operation. Validation studies involve porcine skin with known levels of hydration and human subjects with benchmarks against clinical devices. Here and in other practical scenarios, the soft mechanical properties and compliant construction of the sensor enable intimate coupling to the skin without applied force and hold, to avoid angle or pressure-related sources of variability that degrade the accuracy and repeatability of conventional devices. These same features in form factor and performance allow for routine measurements at nearly any location on the body and on subjects of any age.

This collective set of attributes forms the foundations for devices that allow rapid, accurate assessments of skin hydration and skin barrier function with almost zero user burden. Simple interfaces that leverage smartphone technology suggest potential for frequent use in home settings, as preemptive management of skin disease prior to flares for conditions such as AD or XC. Pilot scale clinical studies illustrate these and other capabilities in tracking improvements in skin hydration associated with application of topical moisturizers onto patients with a range of inflammatory skin conditions. Overall, this system has the potential to improve the quality of care for patients by providing objective and accurate measurements of skin barrier function.

Results and Discussion

System Configurations. The device (Fig. 1*A*, shown here without the battery) is a small, wireless platform designed for noninvasive measurements of the temperature and the thermal transport properties of the skin. The width, length, height, and weight of this example, excluding a battery, are 14.6 mm, 25.6 mm, 1.2 mm, and 193.0 mg, respectively. The system includes a thermal actuator and multisensor (TAS) module interconnected by serpentine traces to form a flexible structure that facilitates soft, intimate contact to the skin with robust mechanical and thermal coupling (*Inset*). Fig. 1*B* presents circuit and block diagrams that highlight the Bluetooth Low Energy (BLE) system on a chip (SoC) for control and wireless data communication to a user interface (UI) (typically on a portable device such as a smartphone). The TAS module consists of a thermal actuator (Joule heating through 221 $\Omega \times 2$ resistors; $R_H \times 2$) and Wheatstone bridge circuits with a pair of negative temperature coefficient thermistors (NTC_+, NTC_-) and a known resistor (R) on each bridge for primary measurement purposes. Another pair of NTCs and bridge circuit serves to compensate for changes in the ambient temperature. A digital on/off switch controlled through the UI enables BLE-connection and activation of a general-purpose input/output (GPIO) pin to source a periodic current (6.8 mA for 10 s, and 0 mA for 50 s in a 1-min cycle) into the thermal actuator. This current generates thermal power (Q = 20.4 mW) at the top surface of the structure and thereby delivers heat to the skin below via thermal diffusion. Transport of heat from the actuator to the NTCs depends upon the thermal properties of the skin, and thus serves as the basis for the measurement of skin hydration. Wheatstone-bridge circuits convert the resistances of the NTCs into corresponding voltages (V_+, V_-) that vary in response to changes in temperature, with an opposite polarity ($\Delta V_+ = -\Delta V_-$). This configuration supports enhanced sensitivity compared to schemes used in conventional implementations of TPS methods. A differential amplifier (AMP) in the BLE SoC further amplifies the voltage differences while eliminating common-mode noise to increase the signal-to-noise ratio (SNR). The subsequent analog-to-digital converter (ADC) samples the voltage, for transmission to the UI via BLE radio communication protocols. A software application transforms the voltages into corresponding temperature values based on a calibration factor. Theoretical models then convert these data into thermal transport properties of the skin, which, in turn, can be used to determine health-related parameters such as the hydration state using appropriate models.

The exploded view schematic illustration in Fig. 1*C* highlights the constituent layers and components of the system: a shell structure formed in a biocompatible silicone material for packaging and thermal insulation; a Li-polymer battery (12 mAh); and a flexible copper-clad polyimide substrate (AP8535R; Pyralux) processed by laser ablation (Protolaser U4; LPKF) to define circuit traces that interconnect the thermal actuator (skin side), NTCs (air side), and the BLE SoC. The shell (*Inset*) creates an air pocket around the TAS module to optimize the flow of heat to the skin-facing side of the device and to thermally isolate this region from the ambient. The miniaturized dimensions of the TAS module (width and length of 0.9 and 2.6 mm, respectively) facilitate proper alignment and compliance with the skin, as needed for accurate measurements. A picture of an encapsulated device adhered to the thenar eminence is in Fig. 1*D*. Assuming that the system performs temperature measurements at a 200-Hz sampling rate, transmits an averaged value every 0.1 s (10 Hz) to the UI, and measures the hydration state over 1 min (actuator off for 50 s, on for 10 s) per day, a 12-mAh battery (*SI Appendix*, Fig. S1) supports an expected lifetime of nearly 10 days. Although the systems presented here do not offer capabilities in wireless recharging, such functionality can be easily included.

Thermal Transport Physics and Applications to Measurements of Skin Hydration. Standard modules for TPS measurements capture the time-dependent difference in temperature (ΔT) for cases when

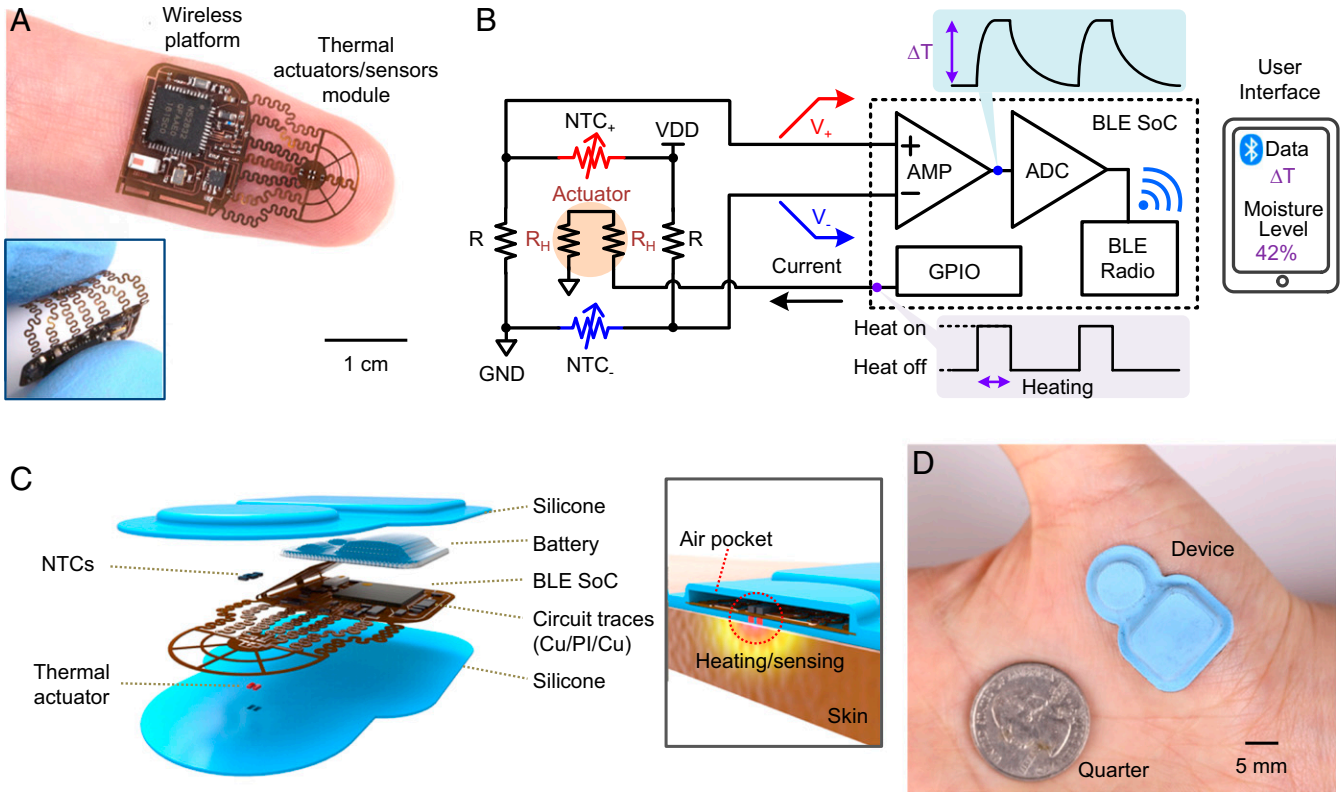

Fig. 1. Soft, skin-interfaced platforms for automatic, wireless sensing of thermal transport properties of the skin. (*A*) Picture of a thin, flexible thermal actuator/sensor (TAS) module integrated with electronics to provide Bluetooth Low Energy (BLE) communication capabilities, resting on the tip of an index finger. The *Inset* features an image of the device bent between the thumb and index finger. (*B*) Circuit and block diagrams of the design. The TAS module consists of a thermal actuator (Joule heater; $R_H \times 2$), and Wheatstone bridge circuits that include two thermistors (NTC_+, NTC_-) with a known resistor (R) on each bridge. A digital on/off switch on the user interface activates a general-purpose input/output (GPIO) pin to source a predetermined periodic current (6.8 mA for 10 s, and 0 mA for 50 s in a 1-min cycle) into the resistive heater. A differential amplifier (AMP) in a BLE system-on-a-chip (SoC) amplifies the difference of the bridge voltages (V_+, V_-). The subsequent analog-to-digital converter (ADC) samples the AMP output voltages for transmission to a smartphone via BLE radio communication. (*C*) Exploded-view illustration of the constituent layers and components: silicone encapsulation layers, battery, and a flexible copper-clad polyimide (Cu/PI/Cu) sheet with circuit traces that interconnect the thermal actuator (skin side), NTCs (air side), and the BLE SoC. The *Inset* highlights an air pocket structure defined by the top silicone encapsulation layer as thermal insulation around the TAS module. (*D*) Picture of an encapsulated device adhered to the thenar eminence.

the thermal actuator is off and on (T_{off} and T_{on}, respectively) (16, 19, 20). The simplest approach to analysis uses a value $\Delta T = T_{on} - T_{off}$ at a single time point, often in a quasi–steady-state regime where the rate of change of temperature with time is relatively small. This parameter then determines an effective thermal transport characteristic, using appropriate models and calibration procedures. Measurement and analysis of the full-time dependence, starting immediately after the actuator is turned on and continuing to the quasi–steady-state regime, can yield substantial information on thermal transport, as described subsequently. In all cases, changes in skin temperature or variable environmental conditions (air currents, ambient temperature fluctuations) that may occur between or during the measurements of T_{off} and T_{on} within a given measurement cycle can affect the value of ΔT, thereby degrading the accuracy and precision of the system. A key feature of the TAS module introduced here (Fig. 2*A*) is that it includes two pairs of NTCs (NTC_1 and NTC_2), as mentioned previously. The primary measurement exploits the difference of the values of ΔT measured from NTC_1 and NTC_2 (ΔT_1 and ΔT_2, respectively; *SI Appendix*, Fig. S2), or $\Delta T_{12} = \Delta T_1 - \Delta T_2 = (T_{on,1} - T_{off,1}) - (T_{on,2} - T_{off,2})$. Here, NTC_2 captures the temperature at a location distant from the thermal actuator, to eliminate the effects of uncontrolled temperature fluctuations, as demonstrated under various conditions in subsequent sections.

An exploded-view illustration of the TAS module (Fig. 2*A*) highlights the constituent layers and components: adhesive (180-μm thickness), thermal actuator (two resistors in series; $R_H \times 2$), NTC_1 (NTC_{1+} and NTC_{1-}), NTC_2 (NTC_{2+} and NTC_{2-}), and silicone encapsulation with air shell. The *Inset* shows a top view of the assembled module. NTC_1 and NTC_2 are directly above and 1.15 mm away from the center of the thermal actuator, respectively. The widths (w) and lengths (l) of both R_H and the NTCs are 0.3 and 0.6 mm, respectively. The compact, dual-sided sensor design (Fig. 2*B*, *Left*) approximately triples the sensitivity (*SI Appendix*, Fig. S3) to the hydration levels of the skin compared to a corresponding single-sided layout (Fig. 2*B*, *Right*). Fig. 2*C* shows the temperature distribution obtained from the finite element analysis (FEA) (*SI Appendix*, Text ST1) induced by operation of the thermal actuator (Q = 20.4 mW) for skin with volumetric composition of 50% of water (k_{skin} = 0.35 $W \cdot m^{-1} \cdot K^{-1}$ and α_{skin} = 0.125 $mm^2 \cdot s^{-1}$; *SI Appendix*, Text ST2) at short (t = 1.0 s; top) and long (t = 10 s; bottom) times following initiation of heating. For a typical epidermal thickness (h = 100 μm), at short times (e.g., t = 1.0 s), thermal transport substantially occurs only through the epidermis. For long times (e.g., t = 10 s), heat passes through the epidermis and significantly into the dermis. Modeling the skin as a bilayer of epidermis and dermis enables extraction of the approximate, averaged hydration level of each layer individually from the ΔT_{12} measurement. At the

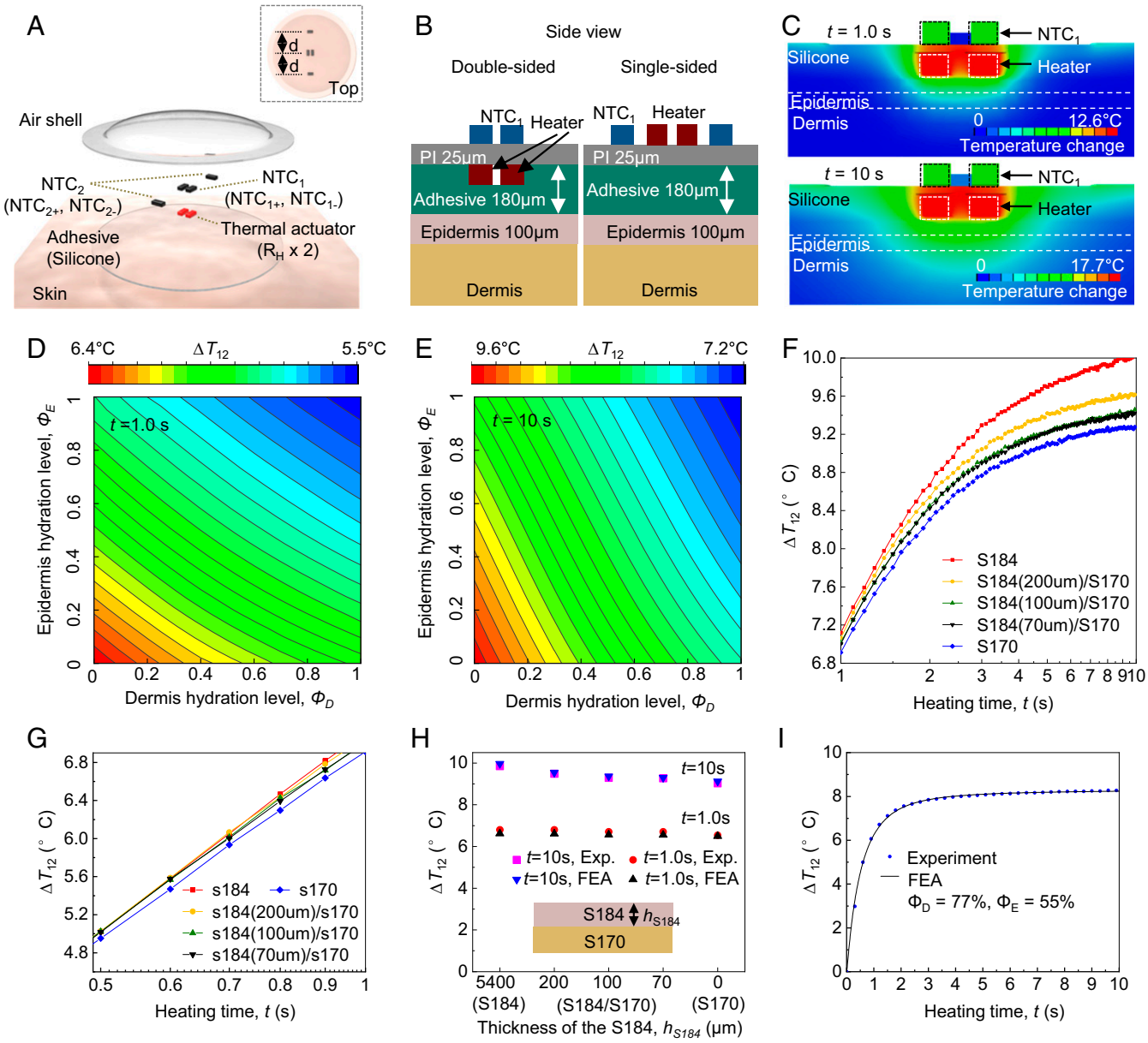

Fig. 2. Finite-element analysis (FEA) of thermal transport throughout the system as the basis for device optimization and data analysis. (*A*) Schematic illustration of the thermal actuator ($R_H \times 2$) with two pairs of thermistors: NTC_1 (NTC_{1+}, NTC_{1-}; resting on the top of the thermal actuator), and NTC_2 (NTC_{2+}, NTC_{2-}; resting at the same distance, *d*, from the actuator). (*B*) Schematic illustration of the FEA model of dual-sided (*Left*) and single-sided (*Right*) sensor designs. (*C*) FEA results for the temperature distribution of the skin with 50% water by volume, at short (t = 1.0 s; *Top*) and long (t = 10 s; *Bottom*) times after initiating thermal actuation (heating power, Q = 20.4 mW). (*D* and *E*) Relationship of ΔT_{12} at short times (t = 1.0 s; *D*) and long times (t = 10 s; *E*) to epidermis (Φ_E) and dermis (Φ_D) hydration levels. $\Delta T_{12} = \Delta T_1 - \Delta T_2$. (*F* and *G*) Wireless measurements of ΔT_{12} at long (*F*; t = 1 to 10 s) and short (*G*; t = 0.5 to 1 s) times for samples that consist of a thick layer of PDMS S184 (red) and S170 (blue), and a thin layer of S184 with different thickness (70 μm, black; 100 μm, green; 200 μm, yellow) on the top of the S170. (*H*) Comparison between FEA and experiment (SD < 3.5%) for PDMS structures described above. (*I*) FEA curve fits of ΔT_{12} (SD < 4.5%) measured for the skin (forearm) throughout the entire measurement period (t = 0 to ~10 s) and the resulting Φ_D and Φ_E.

macroscale, ΔT_{12} (at time t = 0 to ~10 s) can be derived from the thermal properties (thermal conductivity, k; and diffusivity, α) of the epidermis (E) and dermis (D), i.e., k_E, α_E, k_D, and α_D, with a quantitative correlation established via FEA modeling (*SI Appendix*, Text ST1). A microscale model (*SI Appendix*, Text ST2) of hydrated skin defines relationships between k and α, such that the thermal transport problem can be solved with only two parameters to be determined, i.e., the hydration levels Φ_E and Φ_D of the epidermis and dermis, respectively. At short times (e.g., t = 1.0 s), ΔT_{12} is more sensitive to Φ_E than Φ_D (Fig. 2*D*). Conversely, at long times (e.g., t = 10 s), ΔT_{12} is more sensitive to Φ_D than Φ_E (Fig. 2*E*). Analysis at these two time regimes, or throughout the entire measurement period, can yield both Φ_D and Φ_E.

Test structures built with formulations of poly(dimethylsiloxane) (PDMS) that have thermal transport properties similar to those of dehydrated (S184) and hydrated (S170) skin illustrate the key effects. Fig. 2 *F* and *G* show wireless measurements of ΔT_{12} at long (Fig. 2*F*; t = 1 to ~10 s) and short (Fig. 2*G*; t = 0.5 to ~1 s) times, respectively, for samples that consist of a thick layer of S184 (red) and S170 (blue), and a thin layer of S184 (70 μm, black; 100 μm, green; 200 μm, yellow) on top of the S170. At long times (e.g., t = 10 s), heat passes through the top layer (~100-μm thickness) and

substantially penetrates into the bottom substrate. This process leads to similar values of ΔT_{12} for the S184/S170 structures and those of S170. On the other hand, at short times (e.g., $t = 0.5$ to ~1 s; Fig. 2*G*), the heat generated from the device remains confined to the top layer (~100-μm thickness), where ΔT_{12} from the S184/S170 structures are similar to those of S184. *SI Appendix*, Fig. S4 highlights the FEA results and experimental data for samples described above. The FEA results agree well with the experimental values (Exp.) with SDs less than 3.5%, as shown in Fig. 2*H*. These effects support a mode of operation in which analysis of data across different time intervals allow for separate measurements of the hydration of the epidermis and the dermis. Fig. 2*I* represents results for ΔT_{12} from the forearm throughout the entire measurement period ($t = 0$ to ~10 s). The extracted values of Φ_D and Φ_E, are consistent with the expected water content at different skin depths (21). Similar considerations applied to further reduced time intervals allow for separate measurements of the SC and the epidermis. Unless stated otherwise, the studies described in the following use, for simplicity, a single measurement at 10 s (i.e., ΔT_{12} at 10 s) with a single-layer skin model. The reported values of hydration, referred to as Φ ($\Phi = 0$ for dehydrated skin, and $\Phi = 1$ for water;

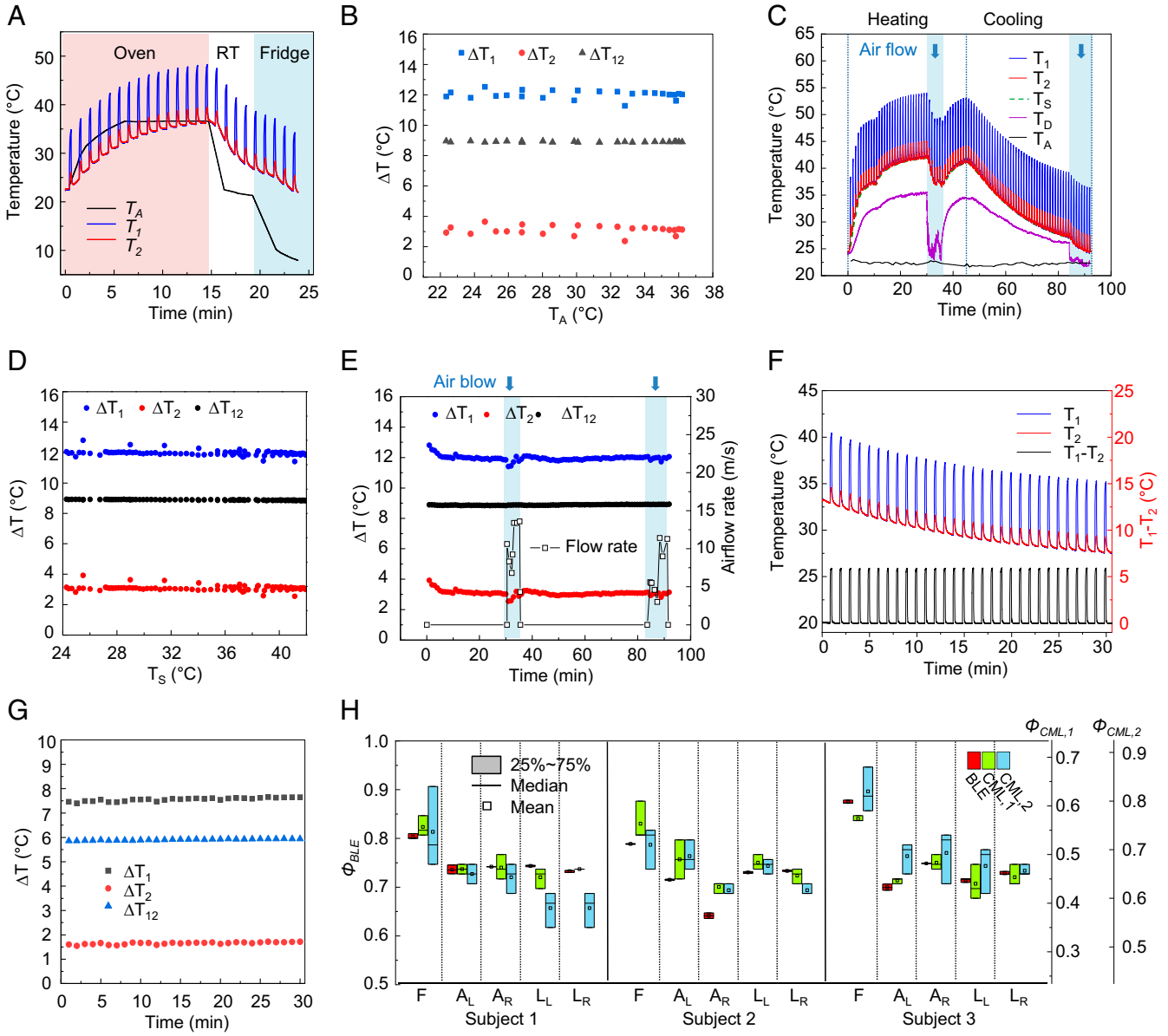

Fig. 3. Experimental studies under various practical conditions. (*A*) Wireless measurements of T_1 (blue) and T_2 (red) in various ambient temperatures (T_A) in an oven and a refrigerator (red and blue background, respectively), and at room temperature (RT). (*B*) Measurements of ΔT_1 (blue), ΔT_2 (red), and ΔT_{12} (black) as a function of T_A. (*C*) Wireless measurements of T_1 (blue), T_2 (red), and substrate temperature (T_S; green dashed line) on/off the hot plate (heating/cooling, respectively) and with different levels of airflow, as a function of time. The surface temperature of the top encapsulation corresponds to that directly above the heating/sensing elements of the device (T_D; purple) and the ambient temperature (T_A; black) was determined using a commercial thermometer. (*D* and *E*) Measurements of ΔT_1 (blue), ΔT_2 (red), and ΔT_{12} (black) as a function of T_A (*D*) and as a function of time (*E*). A pneumatic flow valve controls the flow of air over the device. (*F* and *G*) Wireless measurements of T_1 (blue), T_2 (red), and the difference ($T_1 - T_2$; black) as a function of time (*F*), and of ΔT_1 (blue), ΔT_2 (red), and ΔT_{12} (black) as a function of time (*G*) underwater. (*H*) Skin hydration levels (Φ) measured by three users at the same set of body locations using the BLE device (Φ_{BLE}), and commercial devices for measuring tissue water content ($\Phi_{CML,1}$) and skin surface hydration levels ($\Phi_{CML,2}$). Five different body locations: forehead (F), right arm (A_R), left arm (A_L), right leg (L_R), and left leg (L_L).

SI Appendix, Text ST2), correspond to a weighted average of Φ_D and Φ_E. The measurement characteristics also depend on the layouts and sizes of the thermal actuator and sensor components (as shown in detail in *SI Appendix*, Text ST3).

Experimental Studies. The use of ΔT_{12}, as measured with the two pairs of NTCs (NTC_1 and NTC_2) described previously, minimizes sensitivity to changes in skin temperature or variations in environmental conditions (air currents, ambient temperature, etc.). Demonstrations of the effects involve measurements of samples of S184 in an oven or refrigerator, or on a hot plate as the basis for varying the ambient temperature (T_A; Fig. 3 *A* and *B*) and substrate temperature (T_S; Fig. 3 *C* and *D*), respectively. A pneumatic valve provides control over the flow of air over the device, at rates between 0 and 13.6 m/s (Fig. 3 *C* and *E*). Fig. 3*A* shows wireless measurements of T_1 (blue) and T_2 (red) as a function of time, under conditions of varying ambient temperature, T_A (black), measured using a commercial thermometer (GM 1361; BENETECH). The value of T_A increases from 23.3 to 36.6 °C for 15 min in an oven (red background), and then decreases from 36.6 to 8.0 °C for an additional 9 min in a room temperature ambient (RT; white background) and subsequently in a refrigerator (blue background). Wireless measurements of ΔT_1 (black), ΔT_2 (red), and ΔT_{12} (blue) as a function of T_A are in Fig. 3*B*. The SD for ΔT_{12} across T_A from 8.0 to 36.6 °C is 0.03 °C, roughly 10 times less than that associated with ΔT_1 and ΔT_2 (0.27 and 0.29 °C, respectively). The values of ΔT_1 and ΔT_2 fluctuate with abrupt increases and decreases of T_A at the moment the device enters and exits the oven, respectively (*SI Appendix*, Fig. S8). Fig. 3*C* shows wireless measurements of T_1 (blue) and T_2 (red) as a function of time on a sample with varying temperature T_S (green) across a physiologically relevant range (from 24.2 to 41.0 °C; Fig. 3*D*), and with airflow rates of 0 to ~13.6 m/s (Fig. 3*E*). T_S (green dashed line) is the base temperature measured from NTC_1 while the thermal actuator is off for 50 s every 1-min cycle. For measurements over a period of 90 min, T_S increases from 25.5 to 41.0 °C during the session labeled "heating" and decreases from 41.0 to 24.2 °C during the session labeled "cooling." The surface temperature of the shell structure above the actuator of the device (T_D; purple) changes accordingly (from 23.9 to 35.5 °C and then back to 21.8 °C), and T_A (black) is constant as ~22.2 ± 0.3 °C. Varying the rate of airflow from the top (blue background) leads to abrupt changes in temperatures in the middle and toward the end of the heating and cooling process, respectively. Measurements of ΔT_1 (blue), ΔT_2 (red), and ΔT_{12} (black) as a function of T_S (Fig. 3*D*) and as a function of time with airflow rates of 0 to ~13.6 m/s (Fig. 3*E*) are in Fig. 3 *D* and *E*, respectively. For cases of varying T_S and airflow rates, ΔT_{12} exhibits an SD of 0.03 °C, roughly six times less than that associated with ΔT_1 and ΔT_2 (0.17 and 0.17 °C, respectively), and the SNR, SNR (dB) = $20 \times \log_{10}(\Delta T_{12,mean}/\Delta T_{12,SD}) > 50$ dB (*SI Appendix*, Table S1). The results indicate that the signals are typically >300 times larger than the noise. Fig. 3 *F* and *G* shows the results of T_1 (blue), T_2 (red), and the difference ($T_1 - T_2$;

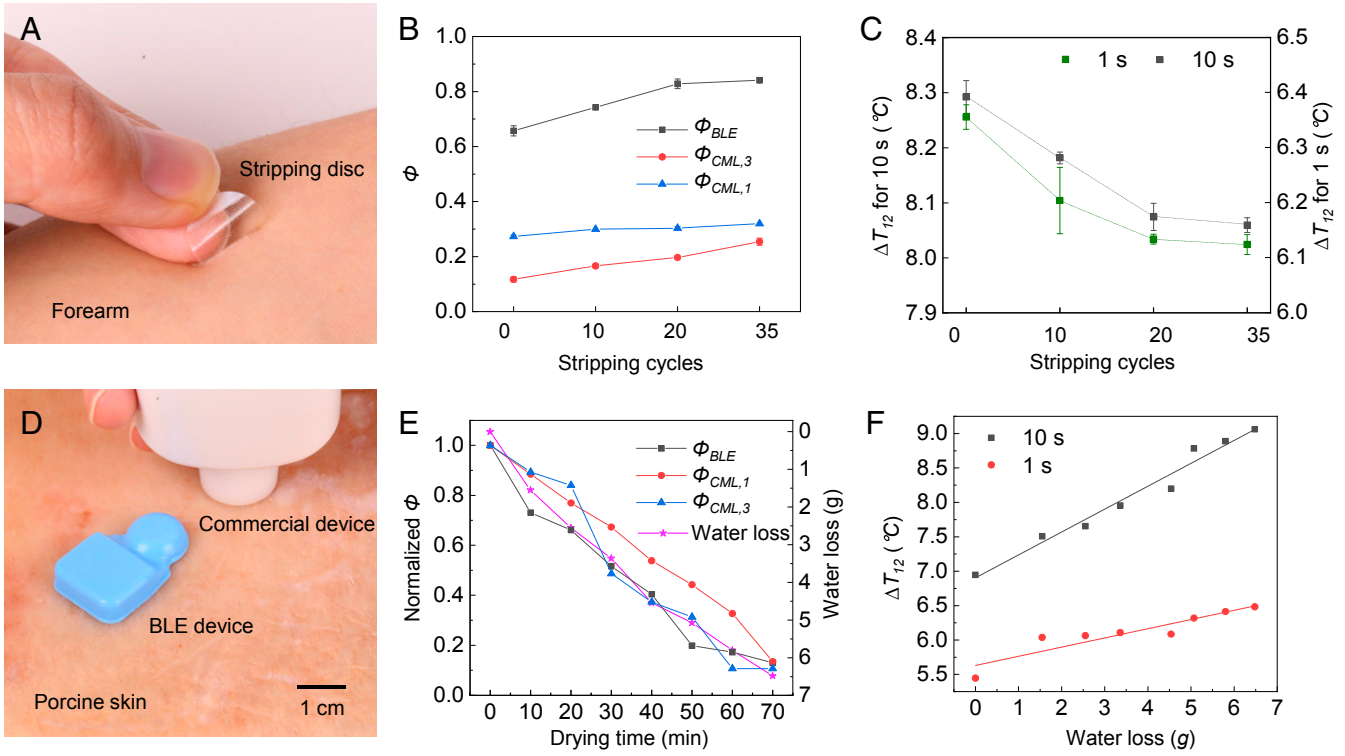

Fig. 4. Experimental studies on the near surface layers of the skin, and on a sample of porcine skin with different, known levels of hydration. (*A*) Optical image of a stripping disk (D-Squame; CuDerm) on the forearm, as a simple and painless means to uniformly remove a fixed area of SC from the skin. (*B*) Measurements of Φ_{BLE} (black) and $\Phi_{CML,1}$ (blue), and SC hydration levels ($\Phi_{CML,3}$; red) measured using a commercial device (MoistureMeterSC; Delfin Technologies) as a function of the number of cycles of adhesive disk stripping. (*C*) Measurements of ΔT_{12} at short (t = 1 s; black) and long (t = 10 s; red) heating times as a function of the number of cycles of stripping. The vertical bar denotes the spread associated with measurements repeated three times. (*D*) Optical image of the device mounted on a sample of porcine skin, next to a commercial device (MoistureMeterSC; Delfin Technologies) for measuring SC hydration levels. (*E*) Measured Φ for a sample of porcine skin with different, known levels of hydration controlled by placing the sample in a food dehydrator (33 °C). (*F*) Measurements of ΔT_{12} (square) and linear fits (solid line) at short (t = 1 s) and long (t = 10 s) heating times for a sample of porcine skin as a function of water loss in grams. The changes in ΔT_{12} exhibit positive correlation with water loss: ΔT_{12} (10 s) = 6.9 + 0.3 × water loss (R^2 = 0.97), and ΔT_{12} (1 s) = 5.6 + 0.1 × water loss (R^2 = 0.85).

black), and ΔT_1 (black), ΔT_2 (red), and ΔT_{12} (blue), respectively, for the case of immersing the device in cooled water (T_S from 33.1 to 27.3 °C). The biocompatible silicone packaging provides robust protection against water penetration such that the SDs of ΔT_1, ΔT_2, and ΔT_{12} over measurement during a 30-min period are 0.07, 0.04, and 0.03 °C, respectively. The hermetic sealing of the devices eliminates the effect of humidity of the surrounding environment on the circuit components.

The devices can laminate gently, without applied pressure, onto the skin for determining Φ via measurements of ΔT_{12}, as described previously. The BLE interface supports wireless, long-range communication to smartphones, with user protocols that require almost no training or specialized skill (Fig. 3*H*). Basic tests involve measurements of Φ at a given body location by three different users from three different healthy subjects using the device reported here (Φ_{BLE}) and commercial (CML) devices for measuring tissue water content ($\Phi_{CML,1}$; MoistureMeterD; Delfin Technologies) and skin surface hydration ($\Phi_{CML,2}$; Gpskin; gpower) via measurements of skin dielectric properties. The measurement depth of the former is 500 to ∼2,500 μm, and that of the latter is 10 to ∼20 μm. The commercial devices require care by the user to hold the probe and manually apply a certain, fixed pressure against the skin for a few seconds for each measurement (*SI Appendix*, Fig. S9). Fig. 3*H* shows the results for Φ at five different body locations (*SI Appendix*, Fig. S10): forehead (F), right arm (A_R), left arm (A_L), right leg (L_R), and left leg (L_L). User variability associated with Φ_{BLE}, $\Phi_{CML,1}$, and $\Phi_{CML,2}$ at the same body location yields an average value of SDs of 0.00, 0.02, and 0.03, respectively. The SDs of $\Phi_{CML,1}$ and $\Phi_{CML,2}$ are the largest (0.04 and 0.09, respectively) on the forehead of subject 2 and 1, respectively, and that associated with Φ_{BLE} is constant (∼0.00) across these five body locations, each with a different curvature and rigidity (*SI Appendix*, Fig. S11). The data show that Φ_{BLE} yields the most repeatable values of Φ. The results for Φ_{BLE} correlate with those from both $\Phi_{CML,1}$ and $\Phi_{CML,2}$ (*SI Appendix*, Fig. S12). Linear fits indicate that $\Phi_{CML,1} = \Phi_{BLE} \times 0.76–0.08$ ($R^2 = 0.76$), and $\Phi_{CML,\,2} = \Phi_{BLE} \times 0.85 + 0.04$ ($R^2 = 0.51$). Bland–Altman plots (difference plots) in *SI Appendix*, Fig. S13 show agreement between readings of Φ calibrated ($\Phi_{BLE,Cal1} = \Phi_{BLE} \times 0.76–0.08$, $\Phi_{BLE,Cal2} = \Phi_{BLE} \times 0.85 + 0.04$) to those from the commercial devices ($\Phi_{CML,1}$ and $\Phi_{CML,2}$). The results show that Φ_{BLE} with calibration yields higher correlation with $\Phi_{CML,1}$ than with $\Phi_{CML,2}$, likely due to the comparable sensing depths for Φ_{BLE} and $\Phi_{CML,1}$.

The measurement is sensitive to the presence and properties of the near surface layers of the skin, including the SC. As a demonstration, Fig. 4*B* shows measurements of Φ_{BLE} and $\Phi_{CML,1}$ (MoistureMeterD; Delfin Technologies) and SC hydration levels ($\Phi_{CML,3}$) determined using a commercial device (MoistureMeterSC; Delfin Technologies; measurement depth of 40 μm) as a function of the number of cycles of applying and removing an adhesive disk (D-Squame; CuDerm; Fig. 4*A*), as a simple and painless means to remove the SC (22). For increasing numbers of cycles, Φ_{BLE} increases in a systematic manner, as evidence of the sensitivity of the measurement to the SC. The data show strong correlations between the values of Φ_{BLE} and the SC hydration levels ($\Phi_{CML,3}$), and number of stripping cycles, while the tissue water content ($\Phi_{CML,1}$) is largely invariant. Values of ΔT_{12} at short ($t = 1$ s) and long ($t = 10$ s) times as a function of stripping cycles, as in Fig. 4*C*, decrease by 3.6% and 2.8%, respectively, after 35 consecutive tape strips. The results indicate that the measurements at short times are more sensitive to the properties of the near surface layers of the skin, consistent with previous discussion of the thermal transport physics.

Studies of a sample of porcine skin (Fig. 4*D*) with different, known levels of hydration are in Fig. 4*E*. The changes in Φ normalized to the value of Φ shortly after placement of the sample in a food dehydrator (33 °C) exhibit strong correlation with independent measurements of the water loss of the sample (see *Methods* for details). Measurements of ΔT_{12} at short ($t = 1$ s) and long ($t = 10$ s) times as a function of water loss are in Fig. 4*F*. The changes in ΔT_{12} exhibit a positive correlation with water loss, as expected: ΔT_{12} (10 s) = 6.9 + 0.3 × water loss ($R^2 = 0.97$), and ΔT_{12} (1 s) = 5.6 + 0.1 × water loss ($R^2 = 0.85$).

Human Subject Evaluations. These miniaturized, flexible platforms can be used on nearly any part of the human body, for adults and children (e.g., hand of a pediatric subject; *SI Appendix*, Fig. S14) alike, including across highly curved or highly sensitive areas of the anatomy. Fig. 5 *A–C* shows photographs of devices mounted on the forehead (Fig. 5*A*), forearm (Fig. 5*B*), and calf (Fig. 5*C*) of a human subject. The *Inset* in Fig. 5*A* features a tilted side view. Studies of hydration levels of the skin of 10 healthy volunteers involve evaluations at five different body locations (*SI Appendix*, Fig. S10): forehead (F), right arm (A_R), left arm (A_L), right leg (L_R), and left leg (L_L). Fig. 5*D* shows ΔT_1, ΔT_2, and ΔT_{12} over a 3-min measurement period from three female (subjects 1, 2, and 9; age range, 25 to 27) and seven male (subjects 3 to 8, 10; age range, 17 to 37) healthy volunteers. The results show that the forehead has the highest hydration level (the lowest values of ΔT_1, ΔT_2, and ΔT_{12}) across all subjects, as expected (23). The values of SDs for ΔT_1, ΔT_2, and ΔT_{12} at each location for all subjects are less than ∼0.06, 0.08, and 0.01 °C, respectively (*SI Appendix*, Fig. S15). The data show that ΔT_{12} yields the most consistent values of Φ, consistent with findings described in the previous sections. Comparisons of Φ from values of ΔT_{12} to those determined with a conventional handheld medical device (MoistureMeterD; Delfin Technologies; *SI Appendix*, Fig. S9) are in Fig. 5*E*. As before, Φ determined using the device introduced here (Φ_{BLE}) correlate strongly with those from the commercial device ($\Phi_{CML,1}$; *SI Appendix*, Fig. S16). Measurements of Φ with calibration coefficients ($\Phi_{BLE,Cal1} = \Phi_{BLE} \times 0.80–0.20$) correspond to $\Phi_{CML,1}$ with an average error (e) of $e = |\Phi_{BLE,Cal1} - \Phi_{CML,1}|/\Phi_{CML,1} = 0.09$ (*SI Appendix*, Fig. S17).

Additional experiments reveal the effect of hair-bearing skin on measurements of ΔT_1, ΔT_2, and ΔT_{12} (*SI Appendix*, Fig. S18). The mean ± SD values of ΔT_1, ΔT_2, and ΔT_{12} over 5-min measurements before and after shaving the skin are 8.76 ± 0.03, 1.78 ± 0.03, and 6.98 ± 0.01 °C (before), and 8.78 ± 0.03, 1.80 ± 0.03, and 6.98 ± 0.01 °C (after), respectively. The effect of perspiration on skin hydration levels before (no sweat), during (sweating), and after (sweat wiped off) a workout appears in *SI Appendix*, Fig. S19. The sweat increases skin hydration levels (Φ_{BLE}) from 0.92 to 0.96 (no wiping)/0.94 (wiping), consistent with previous studies (24, 25).

Evaluation of the Hydration Status of Pathological and Healthy Skin. Water originates from deep epidermal layers and gradually diffuses upward to hydrate cells of the SC, eventually leaving the skin via evaporation at volumes that are comparable to those lost on a daily basis by urination (26). Impaired skin increases this TEWL due to loss of barrier function from desiccation, infection, and mechanical stress (27). The following studies examine changes in the hydration status of disease-affected and clinically unaffected skin. Validation trials involve two patients with AD (subject 1 and 2), a toddler with visibly dry skin (Fig. 6), and three young adults with healthy skin (Fig. 7). Fig. 6 *A* and *B* shows the mounting locations on the back of the hand (atopic eczema), and the forearm (control) of subject 1 (Fig. 6*A*) and on the chest of subject 2 (inflamed, perilesional, and nonlesional skin from *Left* to *Right*; Fig. 6*B*). The *Insets* in Fig. 6 *A* and *B* feature pictures of the forearm of subject 1 after application of moisturizer, and the platform mounted on inflamed (*Left*) and perilesional (*Right*) skin on the chest of subject 2, respectively.

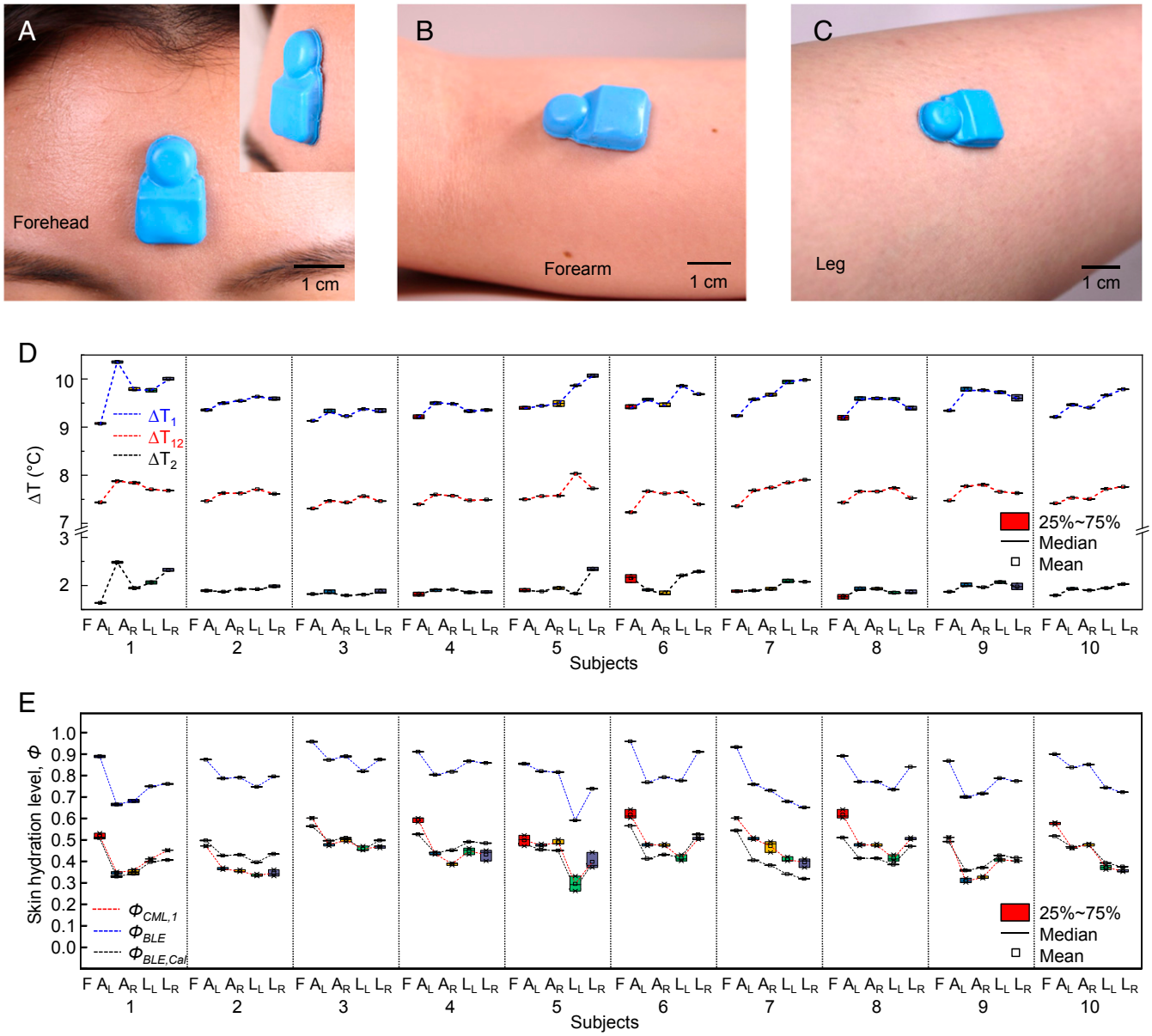

Fig. 5. On-body measurements of skin hydration levels. (*A*–*C*) Pictures of devices mounted on the forehead (*A*), forearm (*B*), and lower leg (*C*) of a healthy female volunteer. (*D*) Wireless measurements of ΔT from NTC_1 and NTC_2, and the differences (ΔT_1, ΔT_2, and ΔT_{12}, respectively) acquired from three female (subjects 1, 2, 9; age range: 25 to 27) and seven male (subjects 3 to 8, 10; age range: 17 to 37) healthy volunteers. Mounting positions on the body: forehead (F), right arm (A_R), left arm (A_L), right leg (L_R), and left leg (L_L). (*E*) Skin hydration level (Φ) from the values of ΔT_{12}, i.e., Φ_{BLE}, and from a commercial medical device, $\Phi_{CML,1}$. The data exhibit strong correlations between Φ_{BLE} and $\Phi_{CML,1}$: $\Phi_{CML,1} = \Phi_{BLE} \times 0.80–0.20$.

The optical image in *SI Appendix*, Fig. S20 shows the platform on the atopic eczema of subject 1, next to a smartphone to collect/display/store the measurements. Results for ΔT_{12} from subjects 1 and 2 are in Fig. 6 *C* and *D*, respectively. Compared with healthy skin (control), lesional skin (eczema in Fig. 6*C*, inflammation in Fig. 6*D*) shows high values of ΔT_{12} and a decrease in ΔT_{12} before and 15 min after (B&A) applying moisturizer, respectively (see *Methods* for details). Fig. 6 *E* and *F* shows the values of Φ from ΔT_{12} (Φ_{BLE}; red) and from MoistureMeterD ($\Phi_{CML,1}$; sky blue) and Gpskin ($\Phi_{CML,2}$; light green), for subjects 1 and 2, respectively. Compared with perilesional and nonlesional skin, atopic eczema and inflammation show low values of Φ_{BLE} (before) and an increase in Φ_{BLE} after application of moisturizer. The tissue water content (values of $\Phi_{CML,1}$) correlates with calibrated values of Φ_{BLE} ($\Phi_{BLE,Cal} = \Phi_{BLE} \times 0.76–0.08$; pink) with an average error (e) of $e = |\Phi_{BLE,Cal} - \Phi_{CML,1}|/\Phi_{CML,1} = 0.09$. The value of $\Phi_{CML,1}$ yields the largest SDs on lesions, lumpy and rigid area (0.03 on atopic eczema and inflamed skin, 0.01 on others), and an average value of SDs of 0.01, larger than that associated with $\Phi_{BLE,Cal}$ (0.00). Moisturizing the skin significantly increases the skin surface hydration level (values of $\Phi_{CML,2}$) up to nearly 1 (0.91 on atopic eczema, and 1.00 on inflamed skin). Fig. 6 *G* and *H* shows the optical images of the device mounted on the forehead (Fig. 6*G*) and the leg (visibly dry skin determined by a dermatologist; Fig. 6*H*) of a toddler (male; age, 2). Measurements of Φ_{BLE} (blue), $\Phi_{CML,1}$ (black), TEWL (red), and SC hydration (SCH; green) on the left leg (LL), right leg (RL), and forehead (FH) are in Fig. 6*I*. The values of TEWL and SCH measured using Gpskin device, and Φ_{BLE} are higher on the

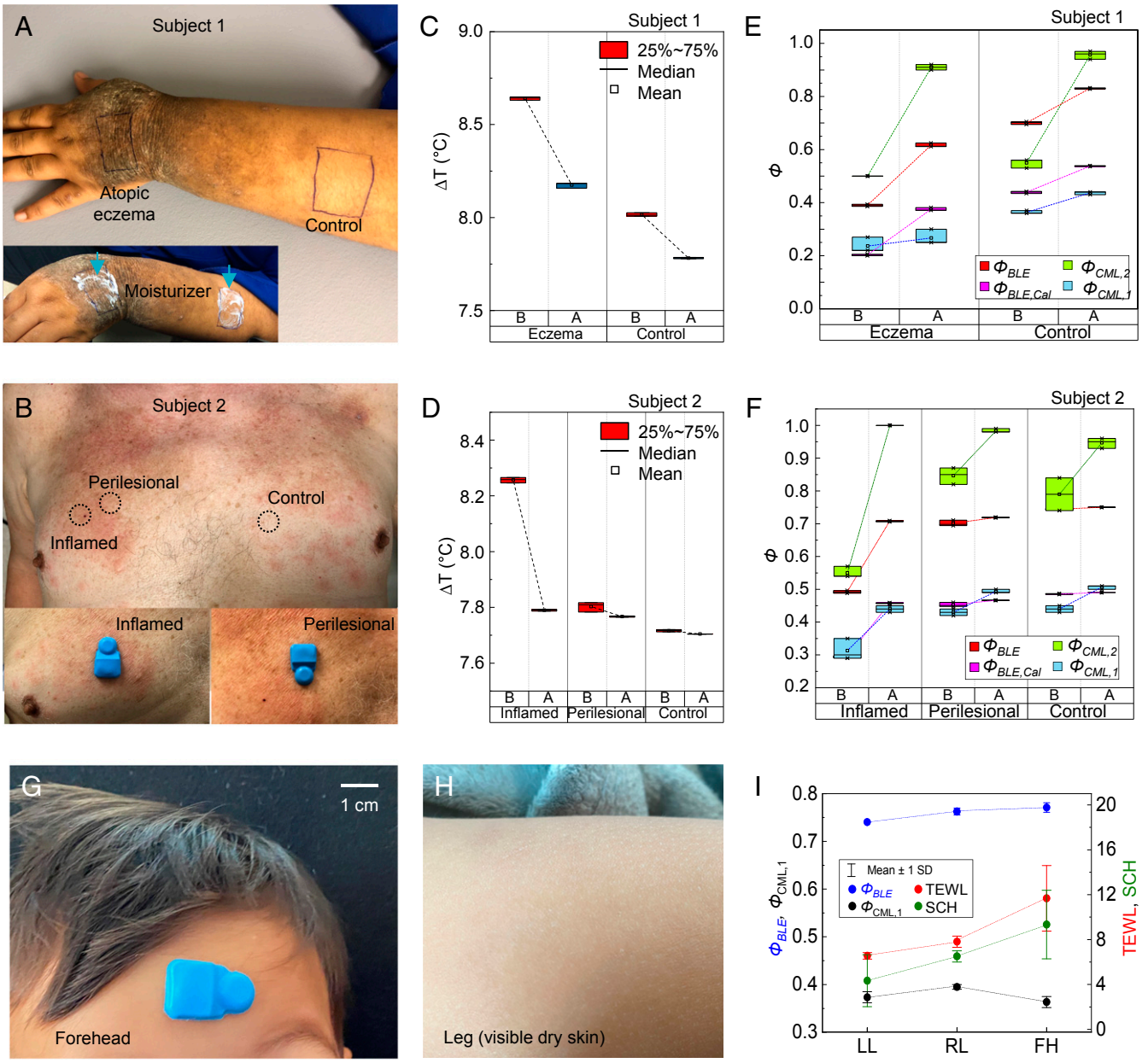

Fig. 6. Wireless measurements of skin hydration on human subjects with atopic dermatitis. (*A* and *B*) Mounting positions on the back of the hand (atopic eczema) and the forearm (control) of a young adult patient with severe AD (subject 1; *A*) and on the chest (inflamed, perilesional, and clinically unaffected skin from *Left* to *Right*) of an elderly patient with inflammatory AD (subject 2; *B*). The studies involve three repeated measurements at each location using wireless and commercial devices before and 15 min after application of moisturizer. The *Inset* shows optical images of the back of the hand, and forearm immediately after application of moisturizer (*A*) and of devices on the inflamed (*Left*; *B*) and perilesional (*Right*; *B*) skin. (*C* and *D*) Wireless measurements of ΔT_{12} before and after (B&A) application of moisturizer from subjects 1 (*C*) and 2 (*D*). (*E* and *F*) Skin hydration level (Φ) measured using commercial devices for measuring tissue water content ($\Phi_{CML,1}$) and skin surface ($\Phi_{CML,2}$) hydration, and from the values of ΔT_{12} (Φ_{BLE}) from subjects 1 (*E*) and 2 (*F*). The results of $\Phi_{CML,1}$ exhibit strong correlations with Φ_{BLE} after calibration ($\Phi_{BLE,Cal} = \Phi_{BLE} \times 0.78–0.08$). (*G* and *H*) Pictures of the device mounted on the forehead (*G*) and leg (*H*; visibly dry skin) of a toddler. (*I*) Measurements of Φ_{BLE} (blue), $\Phi_{CML,1}$ (black), TEWL (red), and SCH (green) on the left leg (LL), right leg (RL), and forehead (FH). The vertical lines denote the error bars.

forehead where the hydration levels are expected to be higher than those on the leg.

Validation trials on three healthy adults (subject 1 with visible dry skin, and subjects 2 and 3 with not visible dry skin determined by a dermatologist) focus on observing variations in Φ after the application of moisturizer (~4 h). The experimental protocol involves five steps: 1) wash the forearm with soap; 2) perform measurements at three different locations ("control," "short," and "long") on the forearm; 3) apply a moisturizer (Extremely Dry Skin Rescue Lotion; Vaseline) on short and long areas, and wait for 1 min on short and 15 min for long; 4) wipe away excess moisturizer from the surface of the skin; and 5) repeat measurements at each location. The changes in Φ_{BLE} and $\Phi_{CML,1}$ normalized to each initial value at the control area are in Fig. 7. The results indicate a strong correlation between Φ_{BLE} and $\Phi_{CML,1}$. Compared to the initial values of Φ_{BLE} at the control area of subject 1 (Fig. 7*A*), the values of Φ_{BLE} at the short (Fig. 7*B*) and long (Fig. 7*C*) areas are 5% and 1% lower,

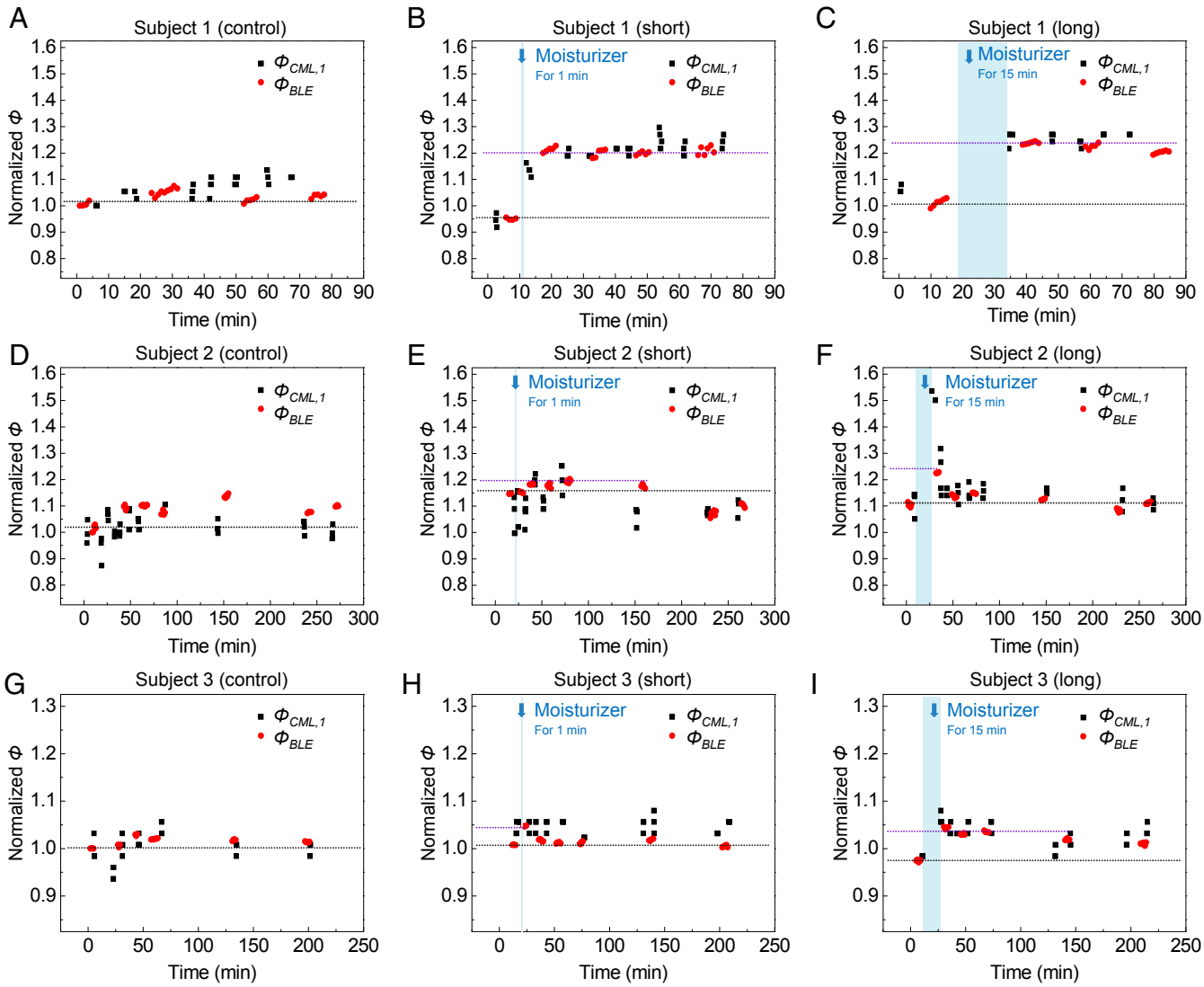

Fig. 7. Studies of the effects of moisturizers on healthy adults. (*A–I*) Changes in $\Phi_{CML,1}$ and Φ_{BLE} from three different skin locations without moisturizer (control; *A*, *D*, and *G*), and 1 min (short; *B*, *E*, and *H*) and 15 min (long; *C*, *F*, and *I*) after application of moisturizer on the forearms of subjects 1 (*A–C*), 2 (*D–F*), and 3 (*G–I*). Measurements are normalized to each initial value determined at time = 0.

respectively, at 0 min, and 20% and 23% higher immediately after the application of the moisturizer. At 80 min, Φ_{BLE} at the long area approaches to a value 20% higher than that at the control area. Compared to the initial values of Φ_{BLE} at the control area of a subject 2 (Fig. 7*D*), the values of Φ_{BLE} at the short (Fig. 7*E*) and long (Fig. 7*F*) areas are 20% and 23% higher after application of the moisturizer, and approach values 10% and 11% higher after ∼4 h. Compared to the initial values of Φ_{BLE} at the control area of a subject 3 (Fig. 7*G*), the values of Φ_{BLE} at the short (Fig. 7*H*) and long (Fig. 7*I*) areas are 5% and 4% higher after application of the moisture, and approach values 0% and 1% higher after ∼3 h. The increase in Φ_{BLE} after applying the moisturizer decreases with time.

Conclusion

The soft, small, wireless platforms reported here enable noninvasive, rapid monitoring of water content of healthy and diseased skin across a wide range of skin conditions, body locations, and subject backgrounds, with accuracy and precision superior to those of existing clinical or research-grade devices. The combined use of an optimized, dual-sided TAS module with multiple, redundant measurement modalities supports repeatable, robust, user-independent measurements under various conditions relevant to practical use in both clinical and home settings. A BLE SoC interface to the phone allows for rapid data acquisition, suitable for operation with minimal training or specialized skills. Full-waveform fitting of the data captured using these systems to bilayer models of thermal transport yields hydration levels for both the epidermis and dermis. Evaluations of skin phantoms and partially hydrated porcine skin validate these measurement and analysis approaches. Pilot scale clinical studies with healthy and diseased subjects (n = 19) illustrate a range of capabilities with clinical relevance. The results define the basis for versatile skin-interfaced devices that can support personalized and localized skin hydration strategies, with potential use as a diagnostic for skin disease states such as AD and XC, as a risk stratification tool for neonates at high risk for the development of AD, and as the basis for objective evaluation of the efficacy of topical medications and personal care product (e.g., topical moisturizers). Additional potential applications include monitoring thermoregulation processes and managing heat-related disorders.

Methods

Fabrication of the Electronics. Prototype devices (Fig. 1) used flexible copper-clad polyimide substrates (AP8535R; Pyralux) processed by laser ablation (Protolaser U4; LPKF), resulting in flexible printed circuit boards (fPCBs) to interconnect surface-mount components, including a BLE SoC (nRF52832; Nordic Semiconductor), resistors (RMCF0201FT; Stackpole Electronics), and temperature sensors (NTC; NCP03XH; Murata). Outcomes of studies of prototype fPCBs served as the basis for designs provided to an ISO-9001 compliant vendor (PCBWay) for final designs. Soldering wire (MM01019; Multicore) and soldering paste (SMDLTLFP10T5; Chip Quik) bonded the BLE SoC to the fPCB by heating at 400 °C, and other various surface-mount components by heating at 190 °C.

Software Development Environment. A BLE mesh kit board (nRF52 DK; Nordic Semiconductor) facilitated development of software for the BLE SoCs. A PC connected to the nRF52 DK with a USB cable for power enabled programming of the on-board BLE SoC. A source-code editor (Visual Studio Code; Microsoft) supported authoring, modifying, compiling, deploying, and debugging software of BLE SoC. A power profiler kit board (NRF6707; Nordic Semiconductor) interfaced with nRF52 DK provided real-time measurements of current consumption of the embedded applications. Android's official integrated development environment (IDE) (Android Studio; Google) provided tools to develop and build the custom Android application (user interface) on smartphones.

Design of the Encapsulating Enclosure. A triple-layered structure of silicone (Ecoflex 00-30; Smooth-On)/silicone gel (Ecoflex gel; Smooth-On), fiberglass fabric (optional, not shown explicitly in Fig. 1), and a different formulation of silicone (Silbione RTV 4420; Elkem Silicones) (80 μm/20 μm/80-μm thickness) served as the bottom encapsulation layer of the device. The bottom adhesive silicone/silicone gel layer provided a direct interface between the heater at the bottom side of the fPCB and the skin, as formed using a three-step process: 1) spin-coating the silicone/silicone gel layer with 2,500 rpm for 30 s on a glass slide and curing on a hot plate at 85 °C for 10 min, 2) gently placing a fiberglass fabric on top of the silicone/silicone gel layer, and 3) spin-coating the following silicone layer with 1,500 rpm for 30 s, placing the device on the uncured silicone layer with the heater side facing down, and curing on a hot plate at 85 °C for 10 min to achieve adhesion between the fPCB and the silicone layer. Curing the silicone (Silbione RTV 4420; Elkem Silicones) inside a custom-made aluminum mold on a hot plate at 85 °C for 20 min formed the top shell of the device (~4-mm height). Curing the top shell and bottom layer together on a hot plate at 85 °C for 20 min with a small amount of silicone (Silbione RTV 4420; Elkem Silicones) as an adhesive sealed the entire system. Cutting the structure using a die cutter completed the fabrication process. Proper cleaning (contaminants/debris removal) using alcohol swipes (Sterile Alcohol Prep Pads; Dynarex) restores the adhesion due to van der Waals forces. Additional adhesives (3M 1524, 3M Tegaderm, etc.) can be used to improve adherence to the skin, as necessary.

Adhesive Stripping Measurement. Repeated application and removal adhesive disks (D-Squame; CuDerm; 14-mm diameter, ~100-μm thickness) several times on the same area of skin gradually removed the SC. Replacement of each disk occurred after five cycles. Measurements after 0, 10, 20, and 35 cycles involved two commercial devices (MoistureMeterSC and MoistureMeterD; Delfin Technologies) and the BLE device.

Porcine Skin Water-Loss Measurement. DPBS solution (Gibco Dulbecco's phosphate-buffered saline; 14190-136; Life Technologies) defrosted a piece of porcine skin (~25-mm thickness; 200 × 100 mm) at room temperature for 12 h. A commercial dehydrator (Sedona Combo Rawfood Dehydrator SD-P9150; Tribest) controlled the hydration level of the porcine skin at 33 °C for 10 min for each measurement. Measured weights of the porcine skin determined with a balance (Ohaus Ax622 Adventurer Precision Balance; Ohaus) enabled a calculation of water loss.

Human Subject Evaluations. The objective was to validate a BLE-based skin hydration monitor as a capable detector of differences in thermal conductivity between dry/hydrated skin and tissue affected and unaffected by skin diseases such as atopic dermatitis. The sensor represents low to minimal risk to the patient, with no electrical component touching the skin. More than 10 healthy control adults/children and 3 patients with mild, moderate, or severe atopic dermatitis were engaged in a dermatology clinic and measured with the sensor by placing it on the skin at discrete locations of the body. The baseline reference for determining TEWL of skin was also obtained using commercially available devices based on capacitance measurements of a dielectric medium in skin.

On-skin tests. Body locations selected for studies included the forehead, left/right forearm, and left/right lower leg. Conventional devices with different probing depths provided baseline references for skin hydration in triplicate on each body location prior to the BLE measurements. A 5-min, continuous measurement using the BLE device were then performed, without the need for a waiting period for the sensor to reach thermal equilibrium with the skin. During the BLE measurements, the subjects were allowed to move freely without any constraint on activities. The tests were performed indoor under an air-conditioned environment.

Moisturizer studies on two patients with AD. The experimental protocol involves four steps: 1) perform three measurements on disease-affected and unaffected skin, 2) apply a moisturizer (Extremely Dry Skin Rescue Lotion; Vaseline) and wait for 15 min, 3) wipe away excess moisturizer from the surface of the skin, and 4) repeat three measurements at each location.

Moisturizer studies on three healthy adults. A thin standardized layer (~1 to 2 g/cm^2) of a commercially available, fragrance-free moisturizer was applied to each location. Repeat measurements were performed at 1 min and 15 min after application of the moisturizer.

Patients (Ann and Robert H. Lurie Children's Hospital of Chicago, Chicago, IL) and healthy/normal subjects (Northwestern University, Evanston, IL) recruited were voluntary and provided full informed consent. This study was approved by the Northwestern University institutional review board (IRB) (IRB study STU00209010). Single-use alcohol wipes (Sterile Alcohol Prep Pads; Dynarex) provided sterilization of the BLE and commercial devices.

Data Availability. All data needed to evaluate the conclusions in the paper are present in the paper and/or *SI Appendix*.

ACKNOWLEDGMENTS. We acknowledge funding from the Querrey-Simpson Institute for Bioelectronics at Northwestern University and from Maruho Company, Ltd., for support of this work.

1. J. Bolognia, J. Jorizza, J. Schaffer, *Dermatology* (Saunders, 2012).
2. J. du Plessis *et al*., International guidelines for the in vivo assessment of skin properties in non-clinical settings: Part 2. Transepidermal water loss and skin hydration. *Skin Res. Technol.* **19**, 265–278 (2013).
3. L. DeSanti, Pathophysiology and current management of burn injury. *Adv. Skin Wound Care* **18**, 323–334 (2005).
4. S. Nutten, Atopic dermatitis: Global epidemiology and risk factors. *Ann. Nutr. Metab.* **66** (suppl. 1), 8–16 (2015).
5. S. Mekić *et al*., Prevalence and determinants for xerosis cutis in the middle-aged and elderly population: A cross-sectional study. *J. Am. Acad. Dermatol.* **81**, 963–969.e2 (2019).
6. M. Kelleher *et al*., Skin barrier dysfunction measured by transepidermal water loss at 2 days and 2 months predates and predicts atopic dermatitis at 1 year. *J. Allergy Clin. Immunol.* **135**, 930–935.e1 (2015).
7. K. Horimukai *et al*., Transepidermal water loss measurement during infancy can predict the subsequent development of atopic dermatitis regardless of filaggrin mutations. *Allergol. Int.* **65**, 103–108 (2016).
8. S. Kezic, J. B. Nielsen, Absorption of chemicals through compromised skin. *Int. Arch. Occup. Environ. Health* **82**, 677–688 (2009).
9. F. L. Filon *et al*., In vitro absorption of metal powders through intact and damaged human skin. *Toxicol. Vitro* **23**, 574–579 (2009).
10. R. Darlenski, S. Sassning, N. Tsankov, J. W. Fluhr, Non-invasive in vivo methods for investigation of the skin barrier physical properties. *Eur. J. Pharm. Biopharm.* **72**, 295–303 (2009).
11. B. Raynor, E. Ashbrenner, M. Garofalo, J. Cohen, F. Akin, The practical dynamics of transepidermal water loss (TEWL): Pharmacokinetic modeling and the limitations of closed-chamber evaporimetry. *Skin Res. Tech.* **10**, 3 (2004).
12. J. C. Cohen *et al*., Comparison of closed chamber and open chamber evaporimetry. *Skin Res. Technol.* **15**, 51–54 (2009).
13. B. Gabard, P. Treffel, "Transepidermal water loss" in *Measuring the Skin*, P. Agache, P. Humbert, Eds. (Springer, Berlin, Germany, 2004), pp. 553–564.
14. V. Rogiers; EEMCO Group, EEMCO guidance for the assessment of transepidermal water loss in cosmetic sciences. *Skin Pharmacol. Appl. Skin Physiol.* **14**, 117–128 (2001).
15. J. Pinnagoda, R. A. Tupker, T. Agner, J. Serup, Guidelines for transepidermal water loss (TEWL) measurement. A report from the standardization group of the European Society of Contact Dermatitis. *Contact Dermat.* **22**, 164–178 (1990).
16. S. Krishnan *et al*., Multimodal epidermal devices for hydration monitoring. *Microsyst. Nanoeng.*, **3** (2017).

17. S. R. Madhvapathy *et al*., Epidermal thermal depth sensors: Epidermal electronic systems for measuring the thermal properties of human skin at depths of up to several millimeters. *Adv. Funct. Mater.* **28**, 1870242 (2018).
18. M. Qassem, V. Kyriacoui, Review of modern techniques for the assessment of skin hydration. *Cosmetics* **6**, 19 (2019).
19. S. E. Gustafsson, Transient plane source techniques for thermal conductivity and thermal diffusivity measurements of solid materials. *Rev. Sci. Instrum.* **62**, 797–804 (1991).
20. T. Okabe *et al*., First-in-human clinical study of novel technique to diagnose malignant melanoma via thermal conductivity measurements. *Sci. Rep*. **9**, 3853 (2019).
21. M. Guzmán-alonso, T. M. Cortazár, Water content at different skin depths and the influence of moisturizing formulations. *Househ. Pers. Care Today* **11**, 35–40 (2016).
22. M. L. Clausen, H. C. Slotved, K. A. Krogfelt, T. Agner, Tape stripping technique for stratum corneum protein analysis. *Sci. Rep.* **6**, 19918 (2016).
23. L. Lünnemann *et al*., Noninvasive monitoring of plant-based formulations on skin barrier properties in infants with dry skin and risk for atopic dermatitis. *Int. J. Womens Dermatol.* **4**, 95–101 (2018).
24. T. Shiohara, Y. Sato, Y. Komatsu, Y. Ushigome, Y. Mizukawa, Sweat as an efficient natural moisturizer. *Curr. Probl. Dermatol.* **51**, 30–41 (2016).
25. T. Shiohara, Y. Mizukawa, Y. Shimoda-Komatsu, Y. Aoyama, Sweat is a most efficient natural moisturizer providing protective immunity at points of allergen entry. *Allergol. Int.* **67**, 442–447 (2018).
26. N. I. Dmitrieva, M. B. Burg, Increased insensible water loss contributes to aging related dehydration. *PLoS One* **6**, e20691 (2011).
27. S. Purnamawati, N. Indrastuti, R. Danarti, T. Saefudin, The role of moisturizers in addressing various kinds of dermatitis: A review. *Clin. Med. Res.* **15**, 75–87 (2017).